NASA TN D-889

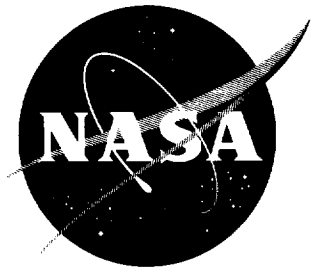

TECHNICAL NOTE

D-889

FREE-FLIGHT AERODYNAMIC-HEATING DATA TO MACH NUMBER 10.4 FOR A MODIFIED VON KÁRMÁN NOSE SHAPE

By William M. Bland, Jr., and Katherine A. Collie

Langley Research Center
Langley Field, Va.

NATIONAL AERONAUTICS AND SPACE ADMINISTRATION
WASHINGTON

May 1961

P

NATIONAL AERONAUTICS AND SPACE ADMINISTRATION

TECHNICAL NOTE D-889

FREE-FLIGHT AERODYNAMIC-HEATING DATA TO MACH NUMBER 10.4 FOR A MODIFIED VON KÁRMÁN NOSE SHAPE[1]

By William M. Bland, Jr., and Katherine A. Collie

L
1
6
1
0

SUMMARY

Aerodynamic-heating data have been obtained on a modified fineness-ratio-5.0 Von Kármán nose shape at free-stream Mach numbers up to 10.4 with a rocket-propelled model. Transient skin temperatures were measured at one station, 26.6 inches behind the tip of a nose 31.6 inches long. A maximum skin temperature of 1,663° R was measured soon after the maximum Mach number was obtained.

During the periods for which experimental Stanton numbers were presented, flow parameters just outside the boundary layer at the temperature measuring station varied as follows: the local Mach number varied in the range between 0.8 and 9.0 and the local Reynolds number varied in the range between 0.8×10^6 and 35.5×10^6. The ratio of skin temperature to local static temperature varied between 1.0 and 3.6.

The experimental Stanton numbers agreed well with Van Driest's turbulent theory while the local Reynolds number was high - that is, while the local Reynolds number varied in a range above 6.8×10^6. For local Reynolds numbers less than 3.5×10^6 the experimental Stanton numbers were of the magnitude predicted by Van Driest's laminar theory. Transition from turbulent to laminar flow at the temperature measuring station, as indicated by the change in the magnitude of the Stanton number, occurred as the local Reynolds number decreased from 6.8×10^6 to 3.5×10^6 at essentially a constant local Mach number of about 9.0.

INTRODUCTION

The problem of aerodynamic heating is currently being investigated by the Pilotless Aircraft Research Division of the Langley Aeronautical Laboratory with techniques that utilize rocket-propelled models in free flight. Results of some recent investigations are presented in reference 1

[1]Supersedes recently declassified NACA Research Memorandum L56D25 by William M. Bland, Jr., and Katherine A. Collie, 1956.

for free-stream Mach numbers up to 3.9 and in reference 2 for free-stream Mach numbers up to 5.6. In these investigations, skin temperatures were measured at single stations on conical noses and on a parabolic nose. Heat-transfer coefficients were obtained from the skin-temperature measurements and compared in the form of Stanton number with theoretical results.

In another investigation, first reported in reference 3, skin-temperature measurements were made at free-stream Mach numbers up to 10.4 at a single station on a modified fineness-ratio-5 Von Kármán nose shape. These skin-temperature measurements have been presented in the form of a time history and compared in reference 4 with calculated skin temperatures based upon the theories of Van Driest.

It is the purpose of this paper to present the aerodynamic-heat-transfer results obtained from the skin-temperature data of the test at a Mach number of 10.4 of references 3 and 4 in the form of local Stanton number. Local Reynolds number, based upon axial distance from nose tip to temperature measuring station, has a maximum value of 35.5×10^6 at a free-stream Mach number of 4.1. The ratio of skin temperature to local static temperature just outside the boundary layer at the temperature measuring station varied from 1.0 to 3.6 during the test.

The flight test was conducted at the Pilotless Aircraft Research Station at Wallops Island, Va.

SYMBOLS

A	area, sq ft
c_f	local skin-friction coefficient
C_H	Stanton number, $\frac{h}{c_{p_v}\rho_v V_v}$
c_p	specific heat of air at constant pressure, Btu/slug-$^\circ$F
c_w	specific heat of wall material, Btu/lb-$^\circ$F
h	local aerodynamic-heat-transfer coefficient, Btu/sec-sq ft-$^\circ$F
J	mechanical equivalent of heat, 778 ft-lb/Btu
k	thermal conductivity of air, Btu-ft/sec-$^\circ$F-sq ft

l	axial distance from nose tip to temperature measuring station, ft
M	Mach number
p	static pressure, lb/in.^{2}
Pr	Prandtl number, $c_p\mu/k$
Q	quantity of heat, Btu
R_v	Reynolds number, $\rho_v V_v l/\mu_v$
R.F.	recovery factor, $(T_{aw} - T_v)/(T_{so} - T_v)$
T	temperature, ^oR
t	time from start of test flight, sec
V	velocity, ft/sec
V_c	velocity of sound, ft/sec
ϵ	emissivity
μ	viscosity of air, slugs/ft-sec (except as noted)
ρ	density of skin material, lb/cu ft; density of air, slugs/cu ft
σ	Stefan-Boltzmann constant, 0.4835×10^{-12} Btu/sq ft-sec-$^oR^4$
τ	thickness, ft

Subscripts:

aw	adiabatic wall
o	static free stream
s	radiation shield
so	stagnation
v	outside boundary layer
w	skin
1,2,3,4	numbers used to identify different heat quantities

MODEL, INSTRUMENTATION, AND TEST

Except for information pertinent to this report, only brief descriptions of the model, instrumentation, and test are presented herein; however, more complete descriptions are presented in reference 3.

Model

The model, which consisted of a modified fineness-ratio-5.0 Von Kármán nose shape, a fineness-ratio-5.0 cylinder, and a frustum of a cone, is shown as a sketch in figure 1 and as a photograph in figure 2. The nose was modified at the tip by the addition of a wedge forward of a station 2 inches behind the tip of the Von Kármán profile.

The nose of the model was machined from stainless steel hollowed out as shown in figure 1. In back of station 7.9, the model had an exterior skin fabricated from 0.032-inch-thick Inconel. The exterior of the nose had a smoothly polished finish. Instrumentation was housed in the nose of the model between stations 9 and 31. A radiation shield made of 0.032-inch-thick Inconel, which was spaced 0.2 inch from the inside surface of the external skin, surrounded the instrumentation to protect it from the high external skin temperatures reached during flight. Increases to the thermal capacity of the external skin were kept to a minimum. As shown in figure 1, the radiation shield joined the external skin at only one station (9.5) between stations 7.9 and 31, and there had a minimum of physical contact.

Instrumentation

Of the six instruments contained in the model, only two were concerned directly with the aerodynamic-heating aspects of the test. Both of these instruments were used to measure temperatures of the external skin at station 25 of the Von Kármán profile (26.6 inches behind nose tip) and both were calibrated in the temperature range from 0° F to 1800° F. One, a thermocouple, was inserted in a hole in the external skin and welded in place, and the other, a resistance wire, was fastened to the inside of the skin with an adhesive. The resistance-wire temperature measuring device failed about 34 seconds after the beginning of the flight test.

Other instrumentation consisted of ground-based radar units for measuring model velocity and for obtaining the position of the model in space. The velocity measuring unit lost the model at about 28 seconds and for times thereafter acceleration and total pressure measured by instruments contained within the model were used to calculate velocity as described in reference 3. A rawinsonde carried aloft by a balloon provided measurements of atmospheric conditions and winds at the time of the flight test.

Test

The desired performance was attained by using a four-stage propulsion system consisting of solid-fuel rocket motors. The model, which contained one of the rocket motors, and the three booster stages are shown in figure 3 as they appeared on the launcher. A portion of the trajectory followed by the model is shown in figure 4, and an altitude time history is shown in figure 5.

DATA REDUCTION

General

During the flight test of the model, measurements furnished the following data, which are basic to the aerodynamic-heating investigation as functions of flight time:

1. Flight-path velocity (fig. 5)

2. Free-stream air density, static air pressure, and velocity of sound (fig. 6)

3. Mach number (fig. 7)

4. Skin temperature (figs. 8 and 9)

5. Free-stream static air temperature (fig. 9)

These data were reduced to Stanton number, the nondimensional form of the local aerodynamic heat-transfer coefficient, by the following procedure. The basic heat-transfer equations as given in reference 5 and used in this procedure are:

For convection,

$$\frac{dQ_1}{dt} = hA_w(T_{aw} - T_w) \tag{1}$$

For radiation (outward),

$$\frac{dQ_2}{dt} = \epsilon_w \sigma A_w T_w^4 \tag{2}$$

For radiation (inward),

$$\frac{dQ_3}{dt} = \frac{\sigma A_w \left(T_w^4 - T_s^4\right)}{\frac{A_w}{A_s}\left(\frac{1}{\epsilon_s} - 1\right) + \frac{1}{\epsilon_w}} \tag{3}$$

Equation (3) applies to the case of coaxial cylinders and is considered to be a good approximation for the coaxial shape used in this investigation.

The time rate of change of heat contained within the skin is

$$\frac{dQ_4}{dt} = \rho_w \tau_w c_w A_w \frac{dT_w}{dt} \tag{4}$$

The sum of the heat transferred to the skin per unit time as expressed by the summation of equations (1), (2), and (3) is equal to the time rate of change of heat contained within the skin

$$\frac{dQ_1}{dt} - \frac{dQ_2}{dt} - \frac{dQ_3}{dt} = \frac{dQ_4}{dt} \tag{5}$$

where the minus sign indicates a loss of heat. Also this expression neglects the conduction of heat along the skin and radiation from outside sources which are estimated to have a negligible effect. Substituting expressions for dQ/dt into equation (5) and solving for the local aerodynamic-heat-transfer coefficient result in the expression

$$h = \frac{c_w \rho_w \tau_w \frac{dT_w}{dt} + \epsilon_w \sigma T_w^4 + \frac{\sigma\left(T_w^4 - T_s^4\right)}{\frac{A_w}{A_s}\left(\frac{1}{\epsilon_s} - 1\right) + \frac{1}{\epsilon_w}}}{T_{aw} - T_w} \tag{6}$$

The local Stanton number can be obtained by nondimensionalizing the local aerodynamic (convective) heat-transfer coefficient, as follows:

$$C_H = \frac{h}{c_{p_v} \rho_v V_v} \tag{7}$$

L 1 6 1 0

Evaluation of Quantities

The properties of the Inconel skin are known. The variation with temperature of the specific heat c_w, as shown in figure 10, was obtained from reference 6. The density ρ_w and thickness τ_w of the skin are known constants, 530 lb/cu ft and 0.00267 foot, respectively. The emissivity of nonoxidized Inconel is shown to vary only slightly from 0.3 over the test range of temperature in reference 6; therefore, ϵ_w and ϵ_s were considered to be equal to 0.3 throughout the test. The time rate of change of the skin temperature dT_w/dt was determined graphically from a suitably scaled time history of the measured skin temperature. The temperature of the radiation shield, which was not measured during the flight test, has been estimated from the unpublished results of some applicable static heating tests and has also been calculated by assuming that all the heat entering the shield was transferred from the external skin by radiation. The estimated and calculated shield temperatures, which are believed to be representative of possible shield temperature limits, are included in figure 11. No significant change in the inward radiation was noted when the different shield temperatures were used in the reduction of the heat-transfer data.

The adiabatic-wall temperature T_{aw} was calculated from the expression for recovery factor (ref. 7)

$$R.F. = \frac{T_{aw} - T_v}{T_{so} - T_v} \tag{8}$$

or rearranging

$$T_{aw} = R.F.(T_{so} - T_v) + T_v \tag{9}$$

For laminar flow R.F. was taken as $Pr^{1/2}$ and for turbulent flow R.F. was taken as $Pr^{1/3}$ as discussed in reference 7, where $Pr^{1/2}$ and $Pr^{1/3}$ were based upon T_w. The variations with temperature of $Pr^{1/2}$, $Pr^{1/3}$, and other thermodynamic properties of air (ref. 8) used in this report are shown in figure 12. In order to account for the variation with temperature of the specific heat of air, the stagnation temperature was calculated with the energy relation

$$\frac{V_o^2}{2J} = \int_{T_o}^{T_{so}} c_p \, dT$$

The local temperature T_v and other local flow parameters at the temperature measuring station have been obtained from the local to free-stream ratios presented in figure 13. These ratios were calculated for the same basic nose shape used in this test, but with a different nose-tip modification. In order to simplify the calculations, the (7.5° half-angle) wedge nose-tip modification to the Von Kármán nose shape of the model was replaced by a 10° half-angle cone that faired smoothly into the Von Kármán nose shape at station 2.7. At supersonic speeds for which $M < 5.0$ the flow-parameter ratios were based upon p_v/p_o ratios calculated by the second-order theory of reference 9. For the rest of the supersonic speed range included in this test, the flow-parameter ratios were calculated by the conical-shock-expansion method of reference 10. No attempt was made to adjust these inviscid flow results for boundary-layer-displacement thickness.

Time histories of the stagnation temperature, adiabatic-wall temperature, free-stream static temperature, and local static temperature at the temperature measuring station are included in figure 9.

ACCURACY

The accuracy of the experimental data as reduced to Stanton numbers has been calculated in the manner described in reference 11. Results of these calculations are as follows:

Time, sec	Possible percent error in C_H
2	±51
4	±24
[a]6	±104
[a]8	±319
[a]10	±114
[a]15	±104
16	±10
18	±4
21	±25
[a]23	±68
24	±17
28	±4
30	±5
34	±9
35	±86
36	±41
38	±19

[a]Data not presented at these times because of the large calculated error.

Examination of these errors and figure 9 shows that the errors in Stanton number become very large when the difference between the adiabatic-wall temperature and the wall temperature becomes small $\left((T_{aw} - T_w) \longrightarrow 0\right)$ and $dT_w/dt \longrightarrow 0$ as between 6 and 15 seconds and near 23 seconds. Also, the calculated errors become large near 35 seconds when $dT_w/dt \longrightarrow 0$.

RESULTS AND DISCUSSION

Local flow parameters at the temperature measuring station, Reynolds number, the ratio of wall temperature to local temperature, and Mach number, are presented as time histories in figure 14.

The skin temperatures as measured by a thermocouple and a resistance wire at a station 26.6 inches behind the nose tip of the model are presented as a function of time in figure 8. The temperatures measured by the two instruments are in very good agreement until shortly before the resistance wire failed at 34 seconds. These data show that changes in skin temperature were very small and thereby indicate little aerodynamic heating until after 16 seconds when acceleration from the second-stage booster increased flight velocity to beyond about $M = 2.0$, corresponding to a local Reynolds number at the temperature measuring station of approximately 20×10^6. It was during the second-stage acceleration that the greatest rate of change of skin temperature was attained, 232° R/sec. The skin temperature continued to increase, except for a short time during the coasting period that followed burnout of the second stage, until a maximum temperature of $1,663^\circ$ R (as measured by the thermocouple) was reached soon after the maximum Mach number of 10.4 was attained. Even though the Mach number after the maximum temperature was still very high, the measured skin temperature started to decrease because the convective heating at the higher altitudes was more than offset by the radiation losses.

By use of the procedure discussed in the section of this report entitled "Data Reduction," the heat-transfer data have been reduced to Stanton number and are presented as a time history in figure 15. In this figure, it can be seen that the Stanton numbers based upon the thermocouple measurements and the resistance-wire measurements are in fairly good agreement. The differences in C_H can be attributed mostly to the differences in slopes of the measured skin temperatures in figure 8. The reduced experimental data have not been presented between 5 and 15 seconds and in the neighborhood of 23 seconds because of the extremely large possible errors calculated for these times as previously noted in the section entitled "Accuracy."

The theories of Van Driest for laminar flow (ref. 12) and for turbulent flow (ref. 13) modified as suggested in reference 14 (p. 16) have been used to calculate the theoretical values of Stanton number for cones and flat plates for the M_V, R_V, and T_w/T_V conditions of the test. The relation $C_{H_{cone}} = \sqrt{3}C_{H_{flat\ plate}}$ was used for laminar flow. For turbulent flow, $c_{f_{cone}}$ was determined from the relation $c_{f_{cone}} = c_{f_{flat\ plate}}$ when $R_{V,cone} = (R_V/2)_{flat\ plate}$ (ref. 15). Values of C_H were then determined from the relation $C_H = 0.6c_f$ (ref. 16). The experimental values of C_H, when compared with theoretical values in figure 15, agreed with the level of turbulent theory to about 32.8 seconds, at which time the local Mach number had increased to the maximum value of 9.0 and the local Reynolds number had decreased to about 6.8×10^6, which was the lowest value since the earliest part of the flight test. After 32.8 seconds the experimental values rapidly decreased until at about 34.5 seconds (at which time M_V had decreased to about 8.9 and R_V had decreased to about 3.5×10^6) they reached a general level slightly below the magnitude predicted by laminar theory. During the rest of the test, as M_V decreased to about 8.4 and R_V decreased to about 0.8×10^6, the experimental values of C_H fell progressively lower than even the laminar flat-plate theory.

In general, the experimental values of C_H do not agree best with either the flat-plate or the conical theory. This was not unexpected because the tested nose shape was neither a cone nor a flat plate and was of such shape that the pressure varied along its surface.

CONCLUDING REMARKS

Aerodynamic-heating data have been obtained at one station, 26.6 inches behind the tip of the nose, on a modified fineness-ratio-5.0 Von Kármán nose shape at free-stream Mach numbers up to 10.4 with a rocket-propelled model. Flow parameters just outside the boundary layer at the temperature measuring station varied as follows: the local Mach number varied in the range between 0.8 and 9.0, the local Reynolds number varied in the range between 0.8×10^6 and 35.5×10^6. The ratio of skin temperature to local static air temperature varied between 1.0 and 3.6.

The experimental Stanton numbers agreed well with Van Driest's turbulent theory while the local Reynolds number was high - that is, while the local Reynolds number varied in a range above 6.8×10^6. For local

Reynolds numbers less than 3.5×10^6 the experimental Stanton numbers were of the magnitude predicted by Van Driest's laminar theory. Transition from turbulent to laminar flow at the temperature measuring station, as indicated by the change in the magnitude of the Stanton number, occurred as the local Reynolds number decreased from 6.8×10^6 to 3.5×10^6 at essentially a constant local Mach number of about 9.0.

Langley Aeronautical Laboratory,
National Advisory Committee for Aeronautics,
Langley Field, Va., April 9, 1956.

REFERENCES

1. Rumsey, Charles B.: Free-Flight Measurements of Aerodynamic Heat Transfer to Mach Number 3.9 and of Drag to Mach Number 6.9 of a Fin-Stabilized Cone-Cylinder Configuration. NACA RM L55G28a, 1955.

2. Rumsey, Charles B., Piland, Robert O., and Hopko, Russell N.: Aerodynamic-Heating Data Obtained From Free-Flight Tests Between Mach Numbers of 1 and 5. NASA TN D-216, 1960. (Supersedes NACA RM L55A14a.)

3. Piland, Robert O.: Performance Measurements From a Rocket-Powered Exploratory Research Missile Flown to a Mach Number of 10.4. NACA RM L54L29a, 1955.

4. Piland, Robert O., and Collie, Katherine A.: Aerodynamic Heating of Rocket-Powered Research Vehicles at Hypersonic Speeds. NACA RM L55E10c, 1955.

5. Eckert, E. R. G. (With Appendix by Robert M. Drake, Jr.): Introduction to the Transfer of Heat and Mass. First ed., McGraw-Hill Book Co., Inc., 1950.

6. Ginnings, Defoe C., and Thomas, Eugenia: The Electrical Resistance and Total Radiant Emittance of Inconel in the Range 0° to 1000° C. NBS Rep. 4111 (NACA Contract S54-52), Nat. Bur. Standards, May 1955.

7. Shapiro, Ascher H.: The Dynamics and Thermodynamics of Compressible Fluid Flow. Vol. II. The Ronald Press Co., c.1954.

8. Keenan, Joseph H., and Kaye, Joseph: Thermodynamic Properties of Air Including Polytropic Functions. John Wiley & Sons, Inc., 1945.

9. Van Dyke, Milton, D.: Practical Calculation of Second-Order Supersonic Flow Past Nonlifting Bodies of Revolution. NACA TN 2744, 1952.

10. Eggers, A. J., Jr., and Savin, Raymond C.: Approximate Methods for Calculating the Flow About Nonlifting Bodies of Revolution at High Supersonic Airspeeds. NACA TN 2579, 1951.

11. Piland, Robert O., Collie, Katherine A., and Stoney, William E.: Turbulent and Laminar Heat-Transfer Measurements on a 1/6-Scale NACA RM-10 Missile in Free Flight to a Mach Number of 4.2 and to a Wall Temperature of 1400° R. NACA RM L56C05, 1956.

12. Van Driest, E. R.: Investigation of Laminar Boundary Layer in Compressible Fluids Using the Crocco Method. NACA TN 2597, 1952.

13. Van Driest, E. R.: The Turbulent Boundary Layer for Compressible Fluids on a Flat Plate With Heat Transfer. Rep. No. AL-997, North American Aviation, Inc., Jan. 27, 1950.

14. Van Driest, E. R.: The Turbulent Boundary Layer With Variable Prandtl Number. Rep. No. AL-1914, North American Aviation, Inc., Apr. 2, 1954.

15. Van Driest, E. R.: Turbulent Boundary Layer on a Cone in a Supersonic Flow at Zero Angle of Attack. Jour. Aero. Sci., vol. 19, no. 1, Jan. 1952, pp. 55-57, 72.

16. Rubesin, Morris W.: A Modified Reynolds Analogy for the Compressible Turbulent Boundary Layer on a Flat Plate. NACA TN 2917, 1953.

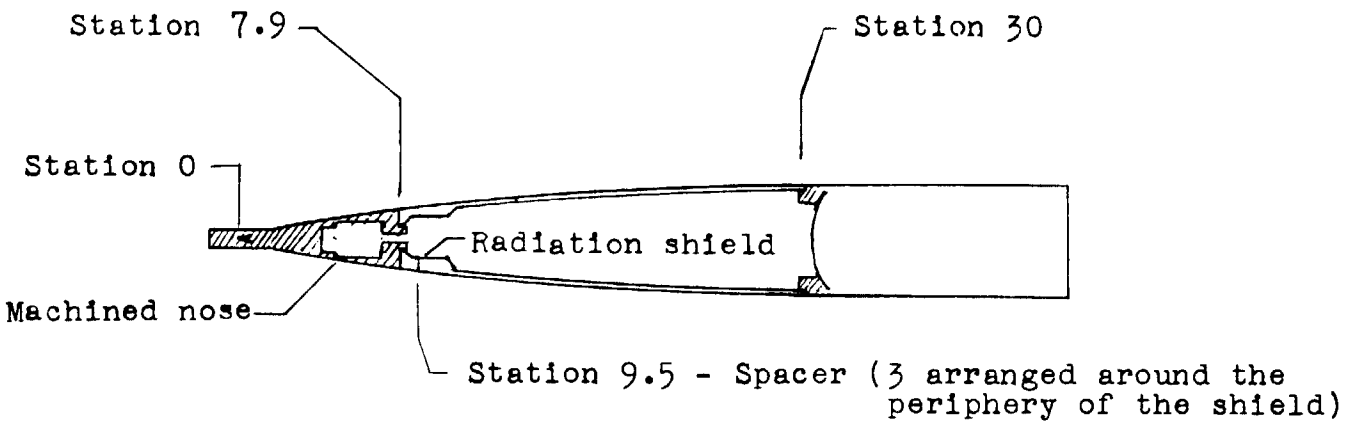

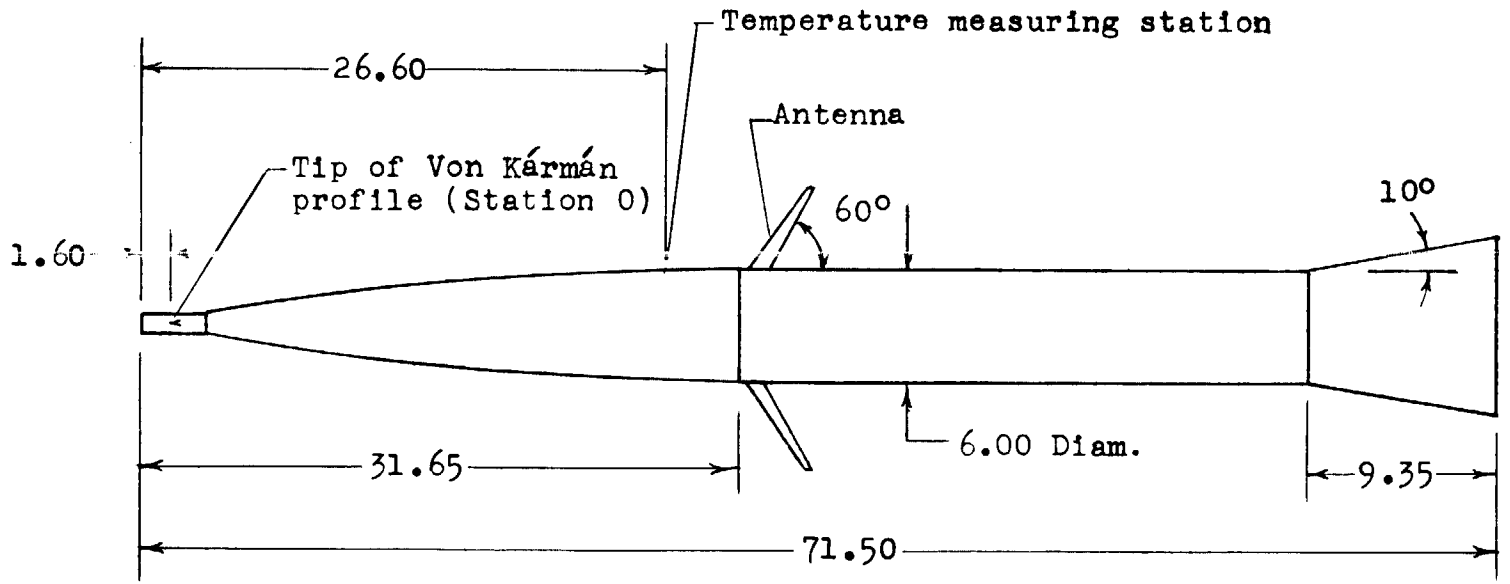

Figure 1.- Sketch of model and detail of nose construction. All linear dimensions in inches.

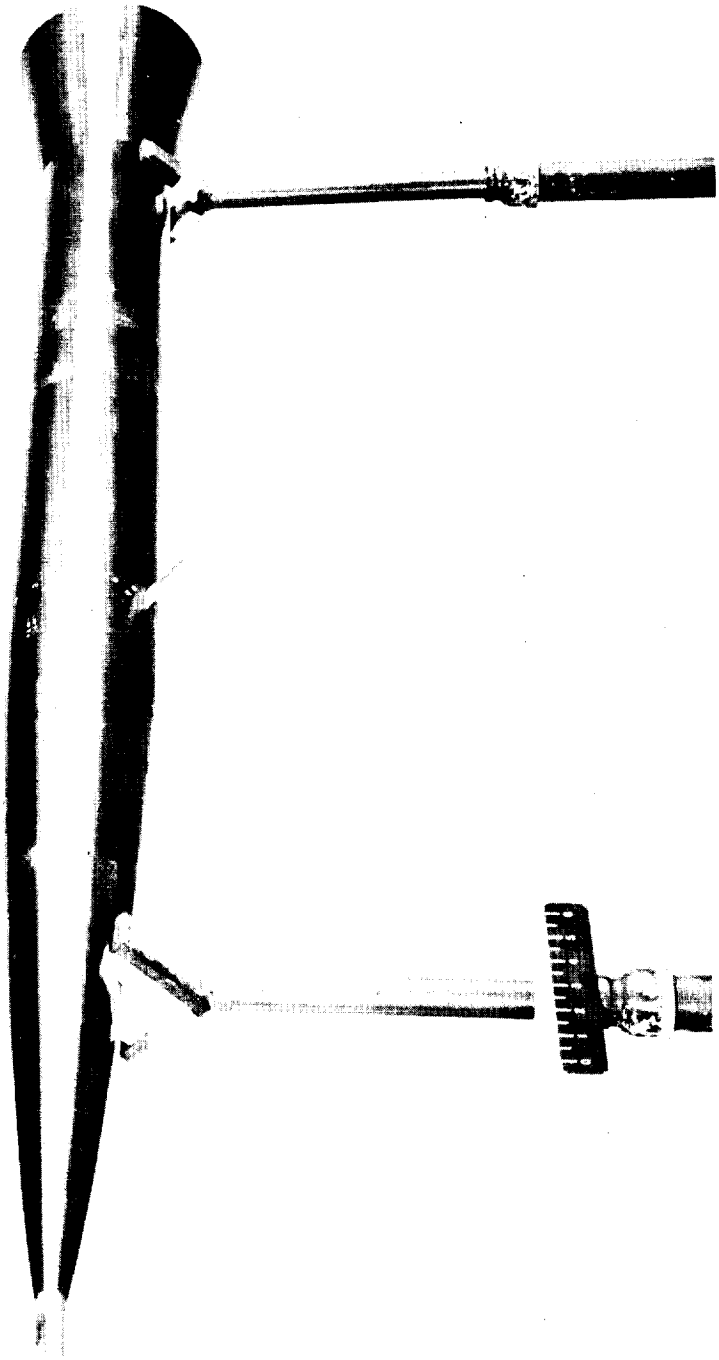

L-86949.1

Figure 2.- Photograph of model.

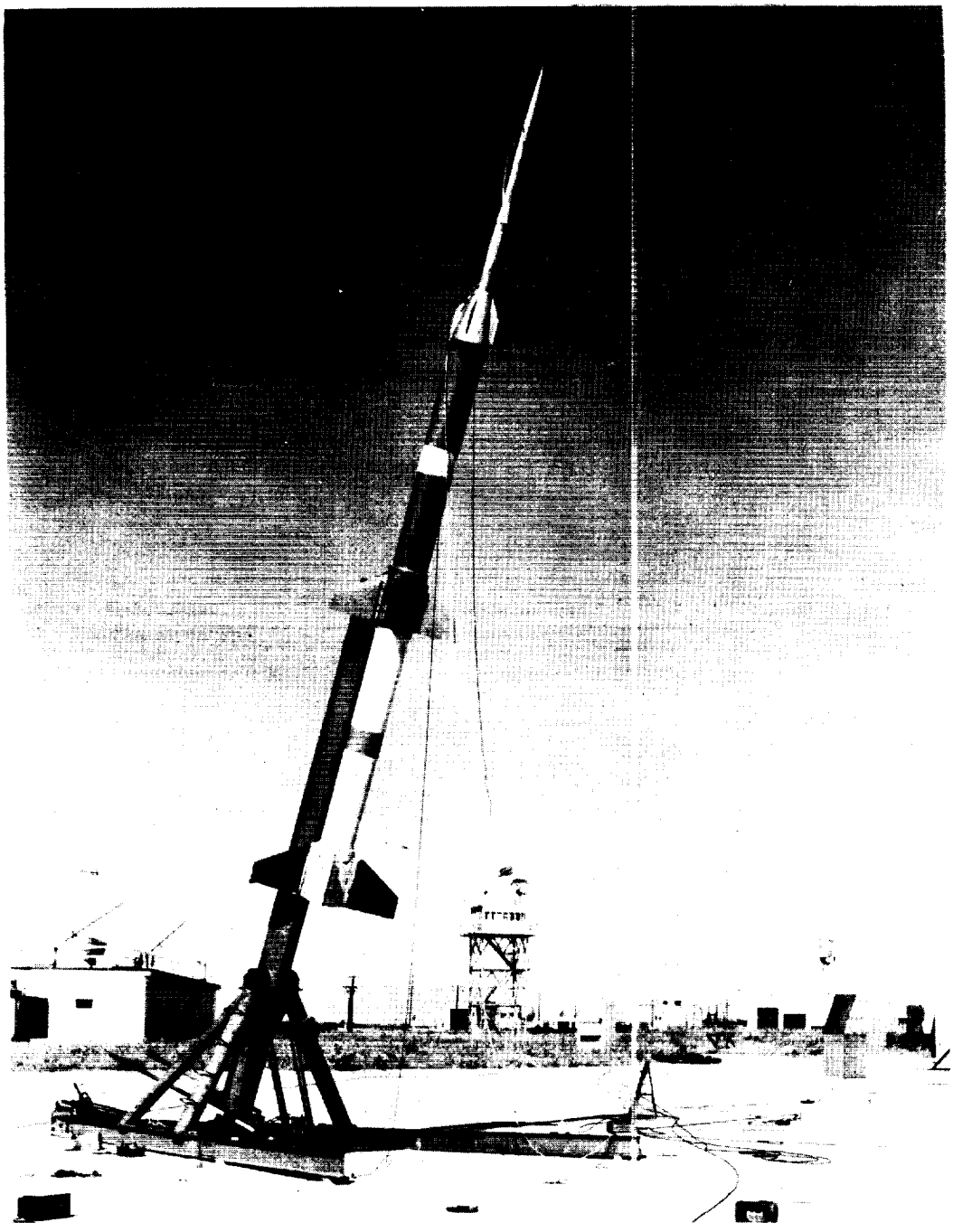

Figure 3.- Model and boosters on launcher. L-87014

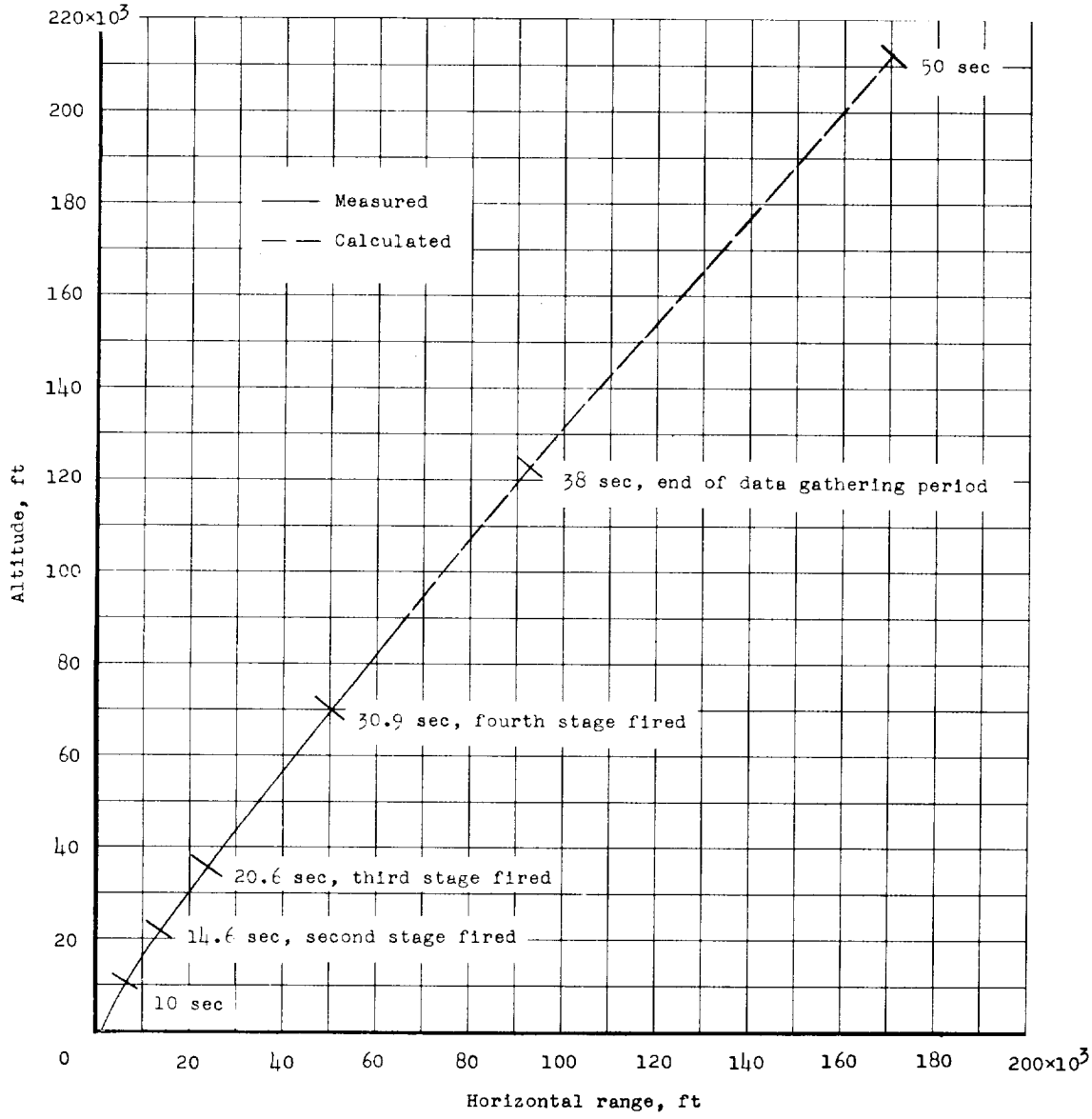

Figure 4.- A portion of the trajectory followed by model.

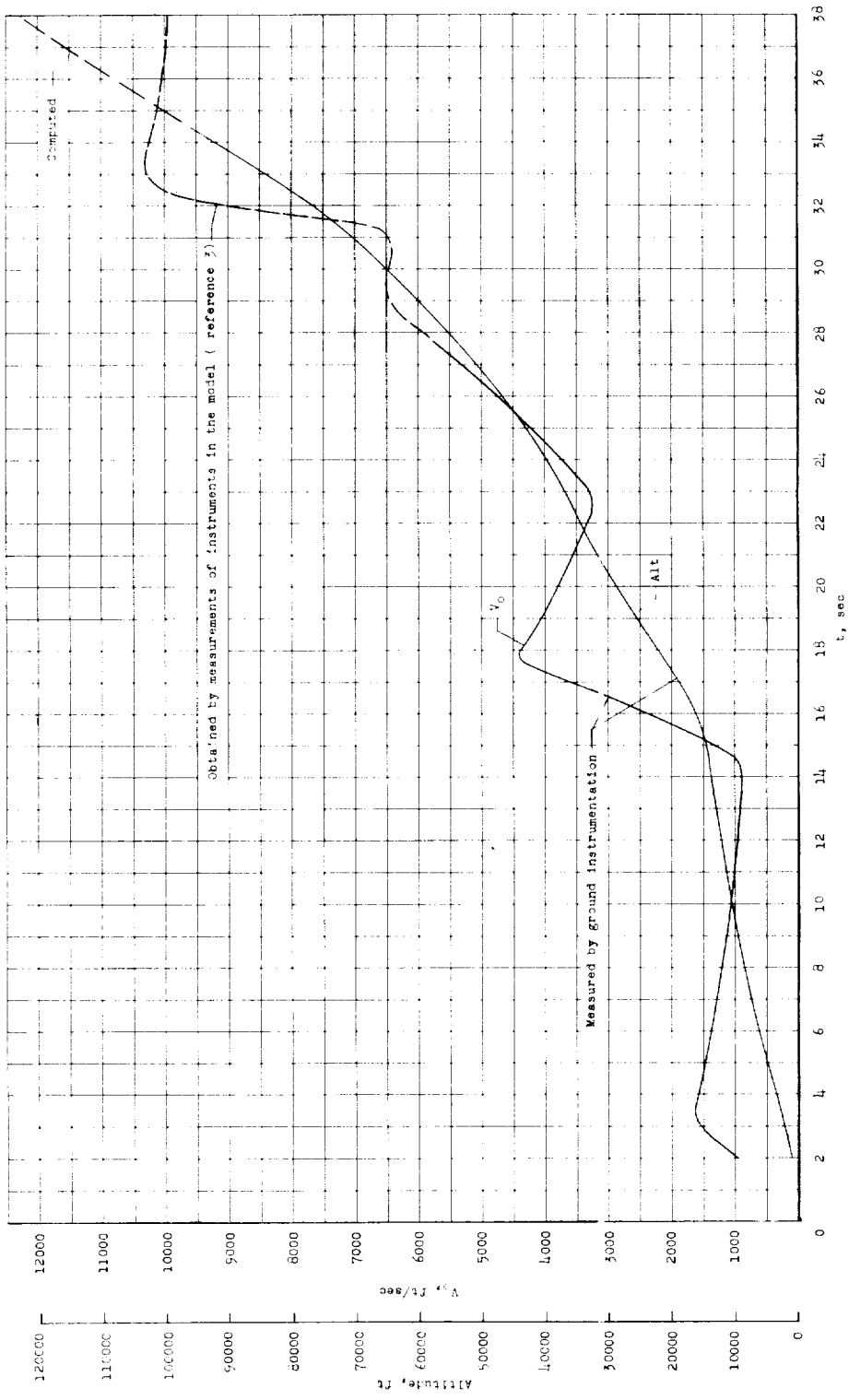

Figure 5.- Time histories of the flight-path velocity and altitude.

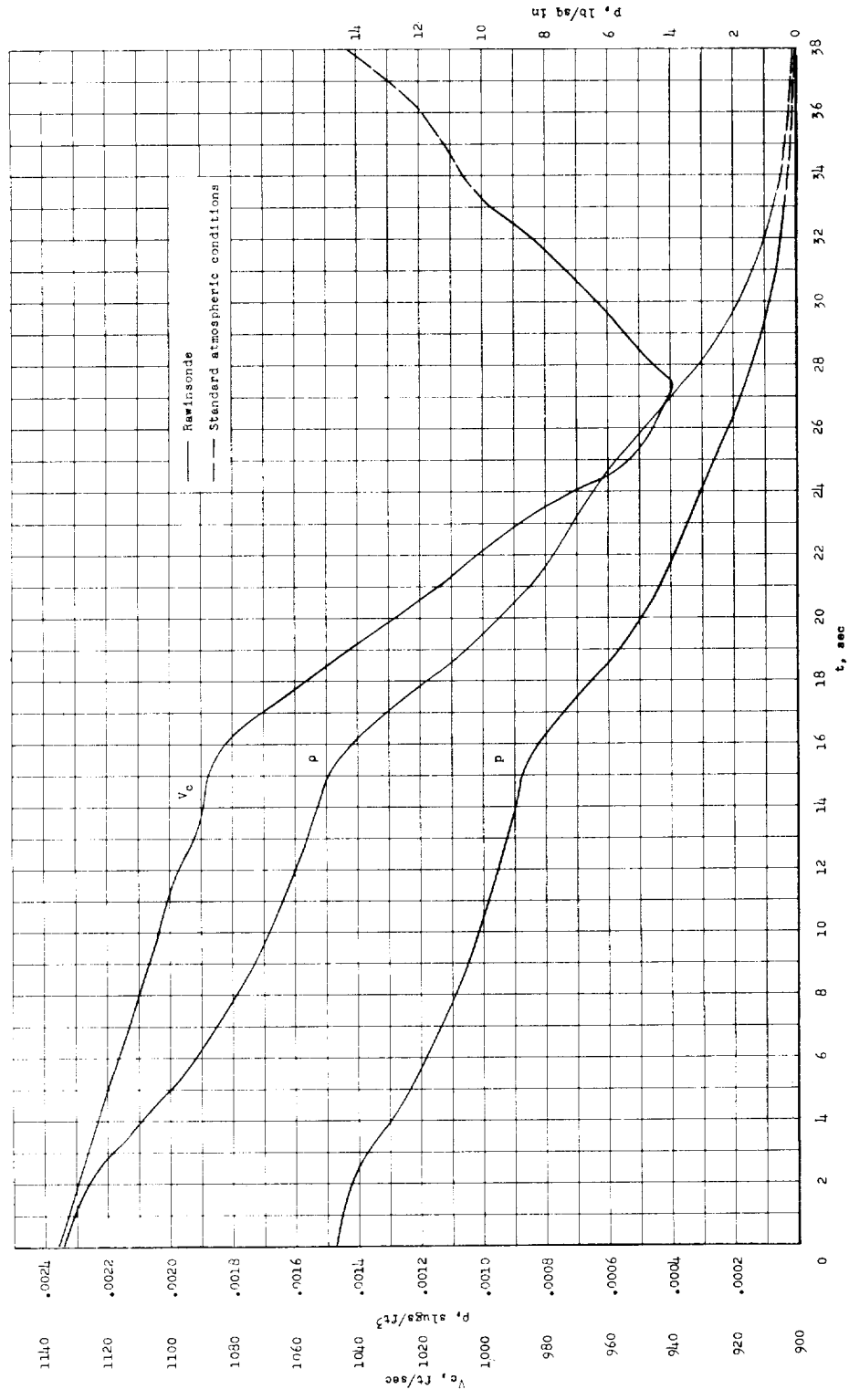

Figure 6.- Time histories of the velocity of sound, density of air, and the static air pressure.

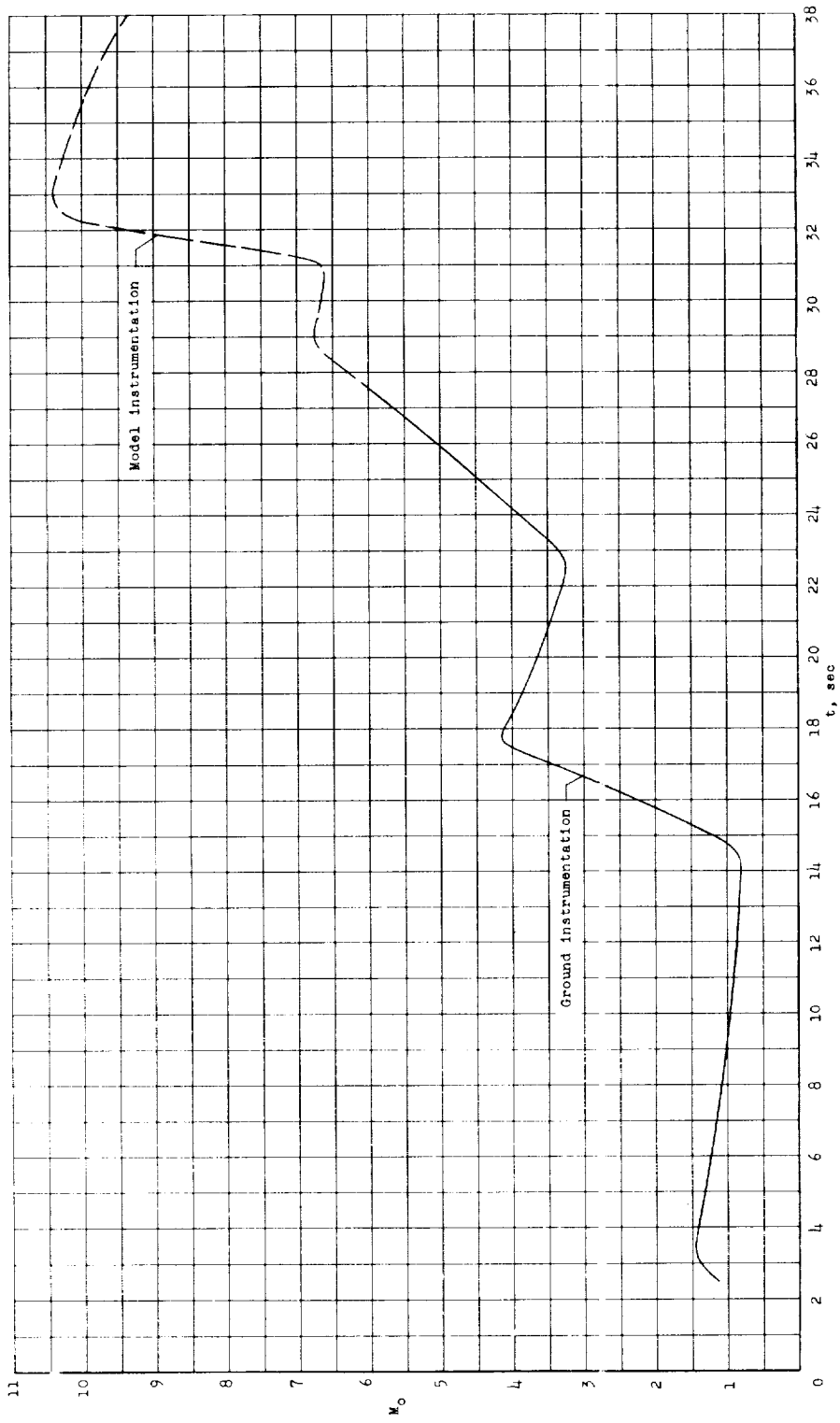

Figure 7.- Time history of the Mach number.

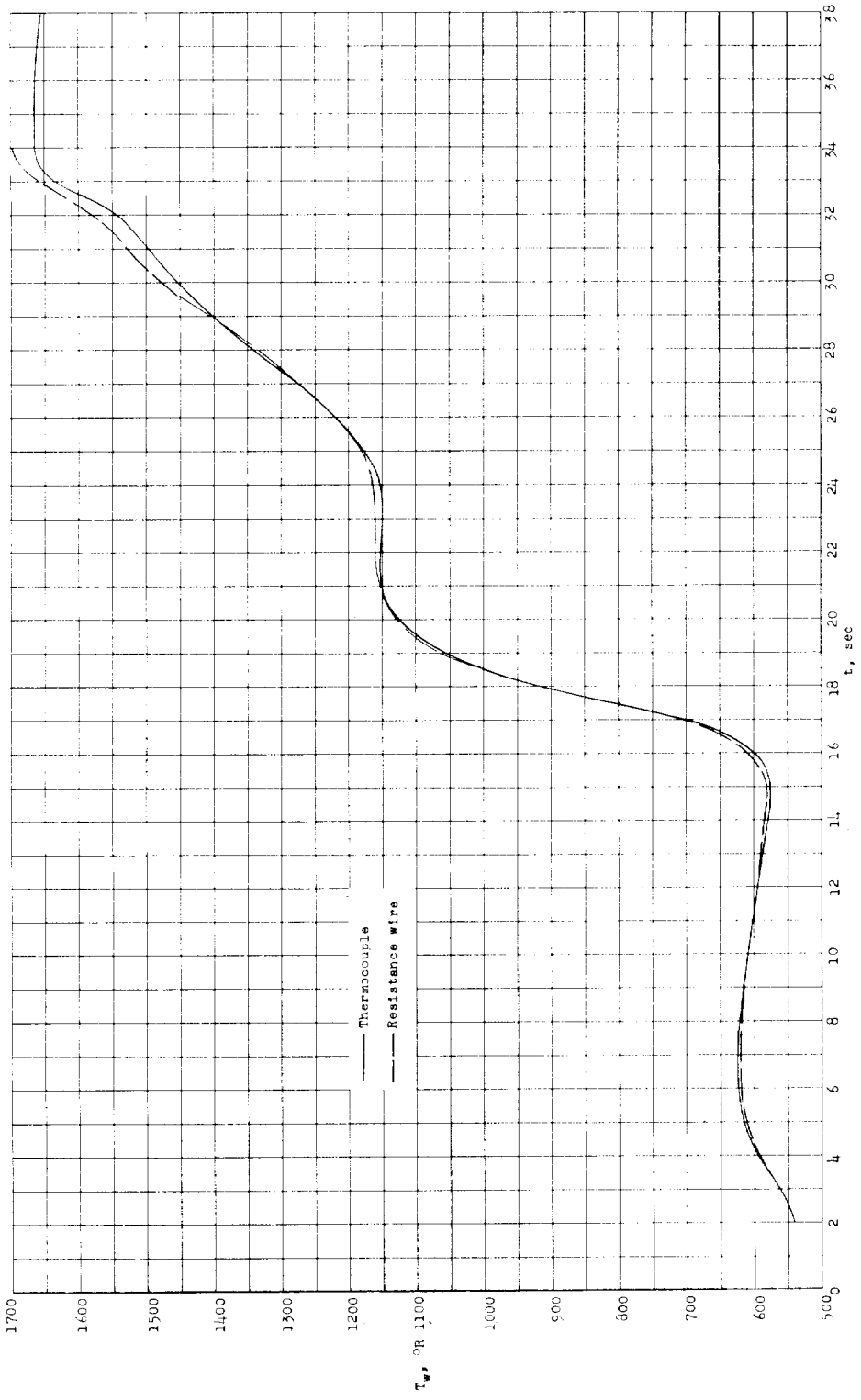

Figure 8.- Comparison of the skin temperatures measured by the thermocouple and by the resistance wire.

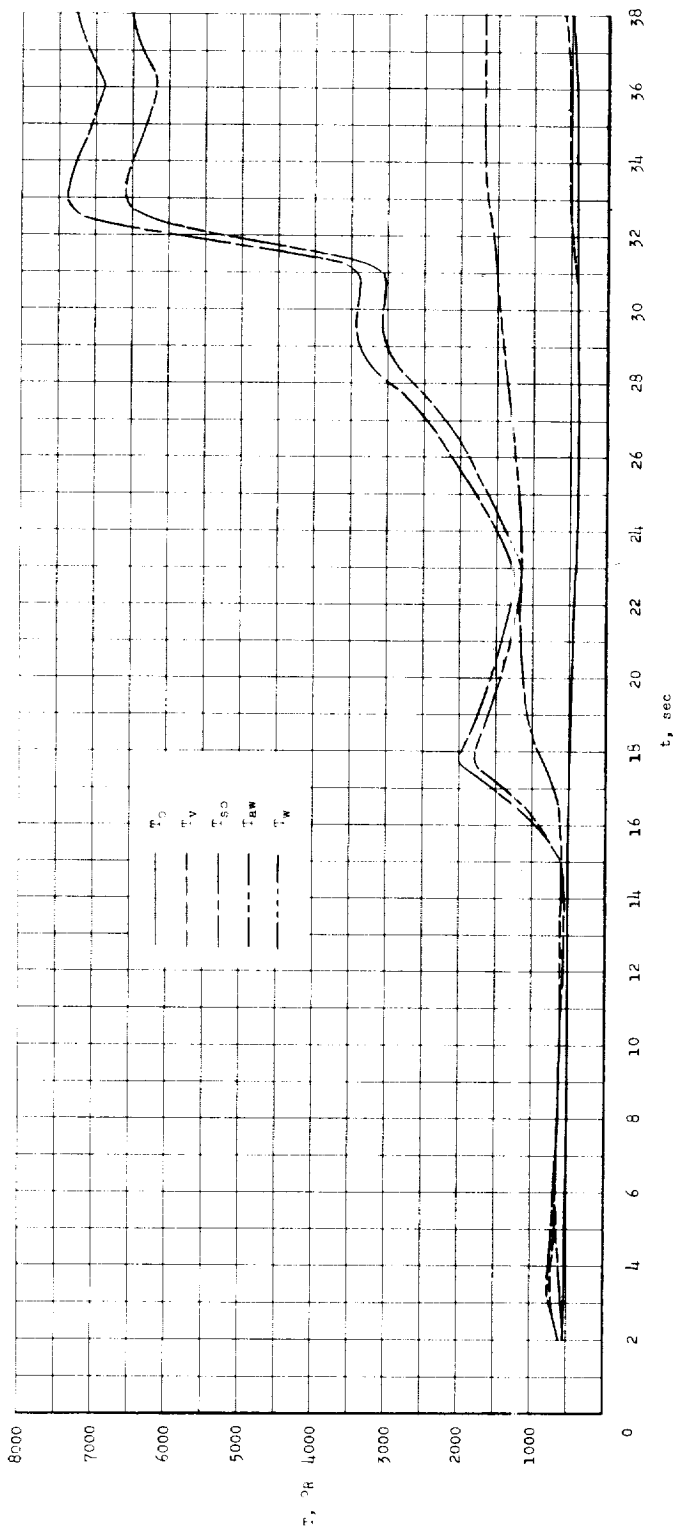

Figure 9.- Time histories of various temperatures.

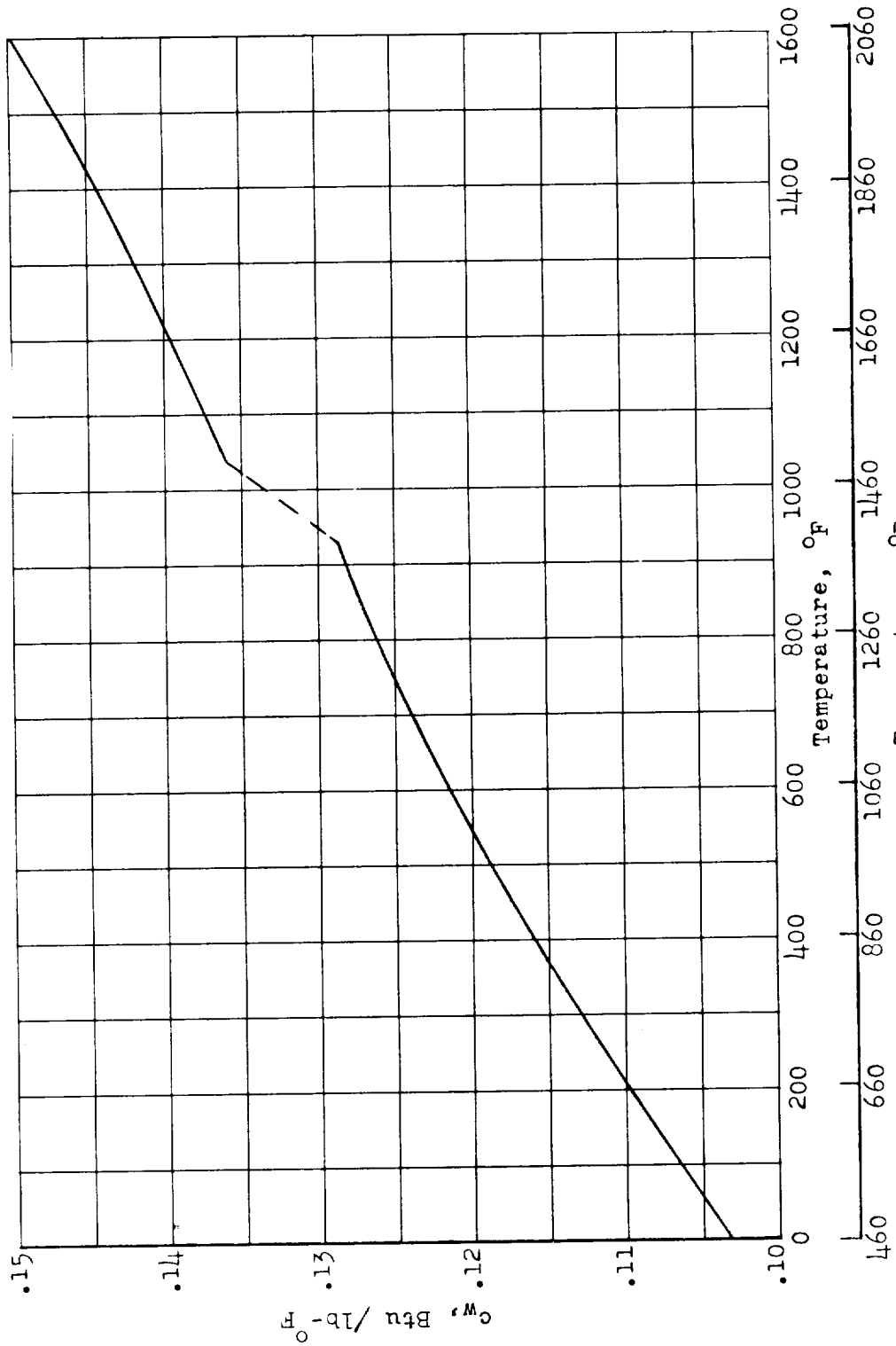

Figure 10.- Instantaneous specific heat of Inconel. (See ref. 6.)

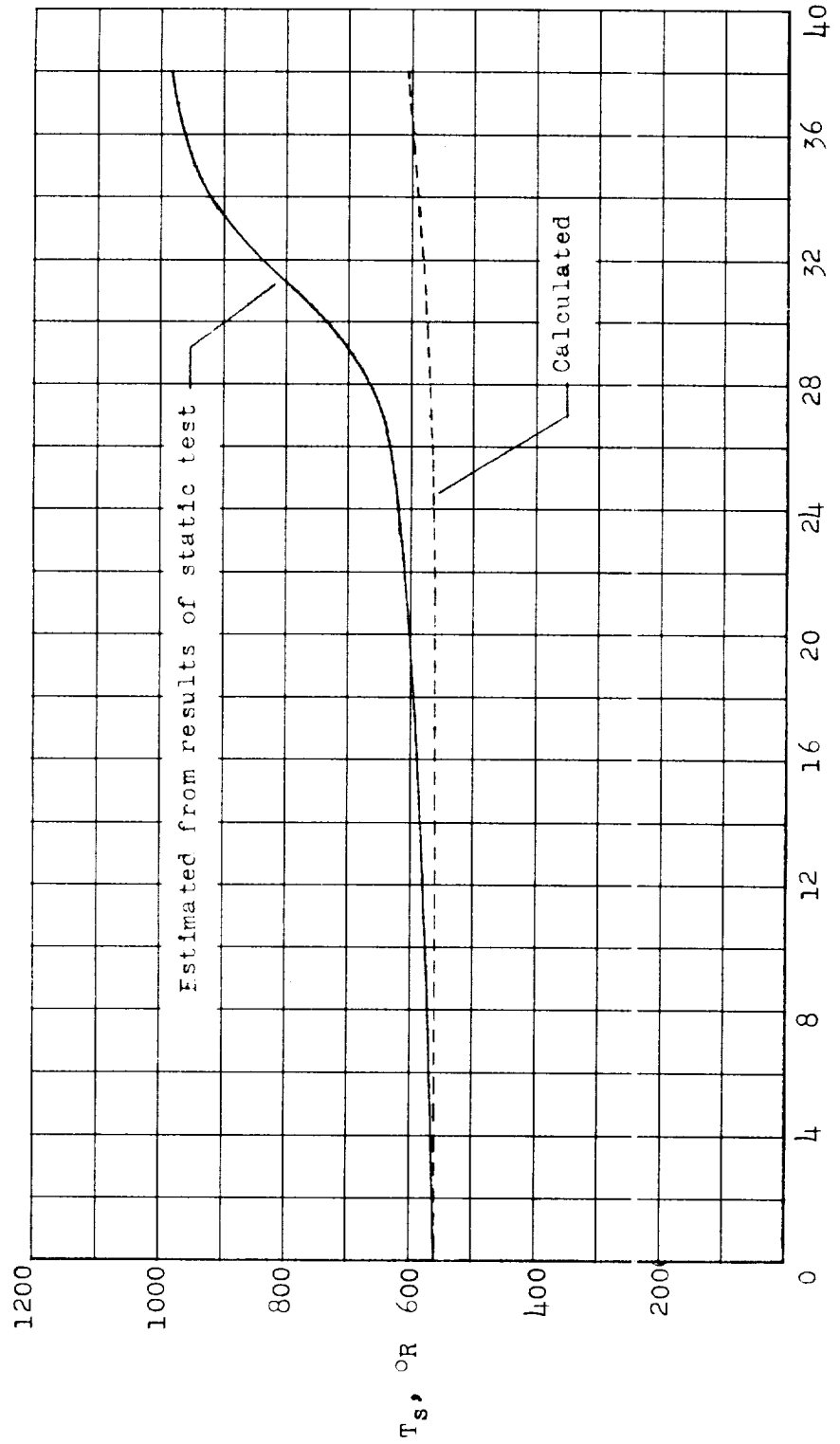

Figure 11.- Variation of shield temperature with time.

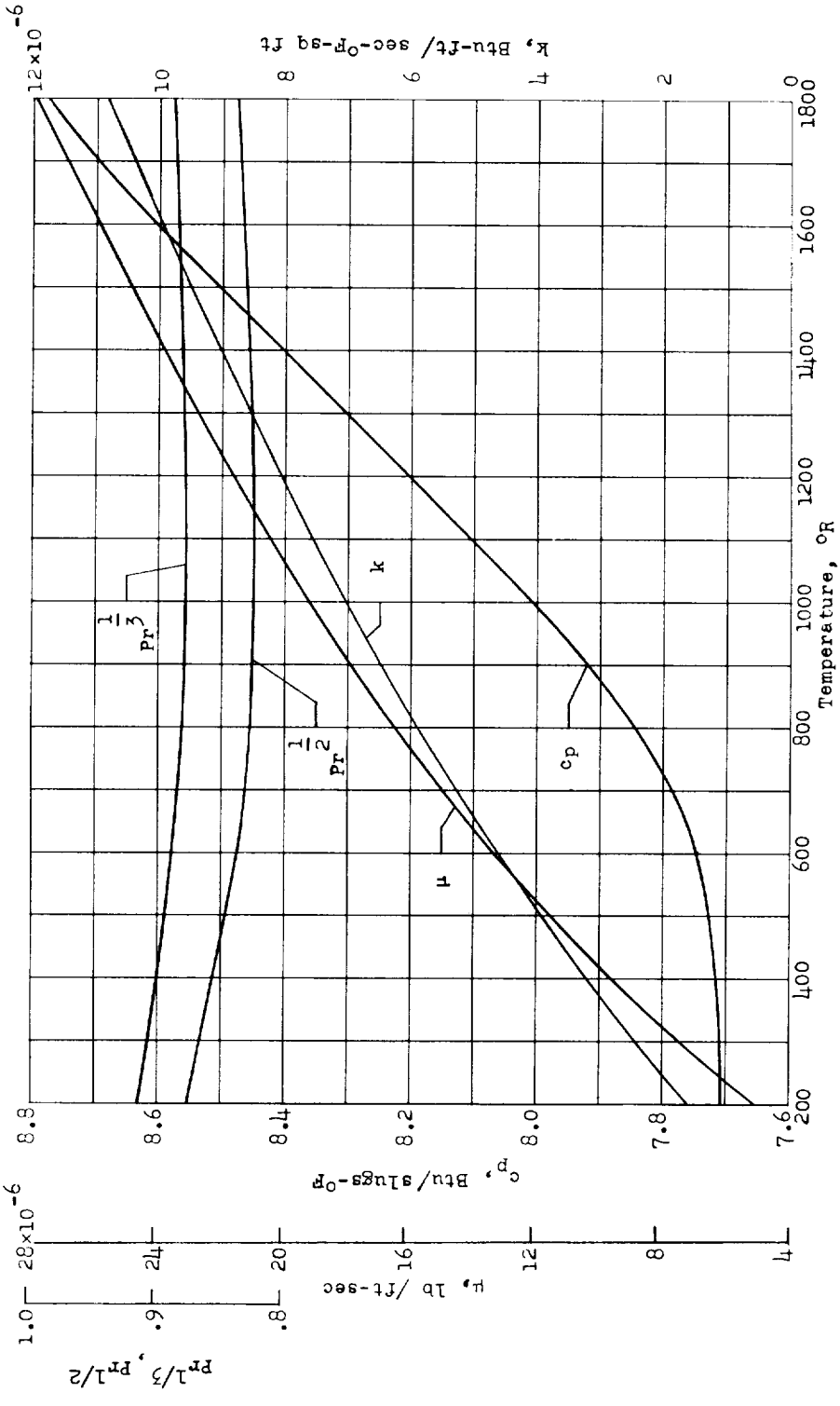

Figure 12.- Thermal properties of air. (See ref. 8.)

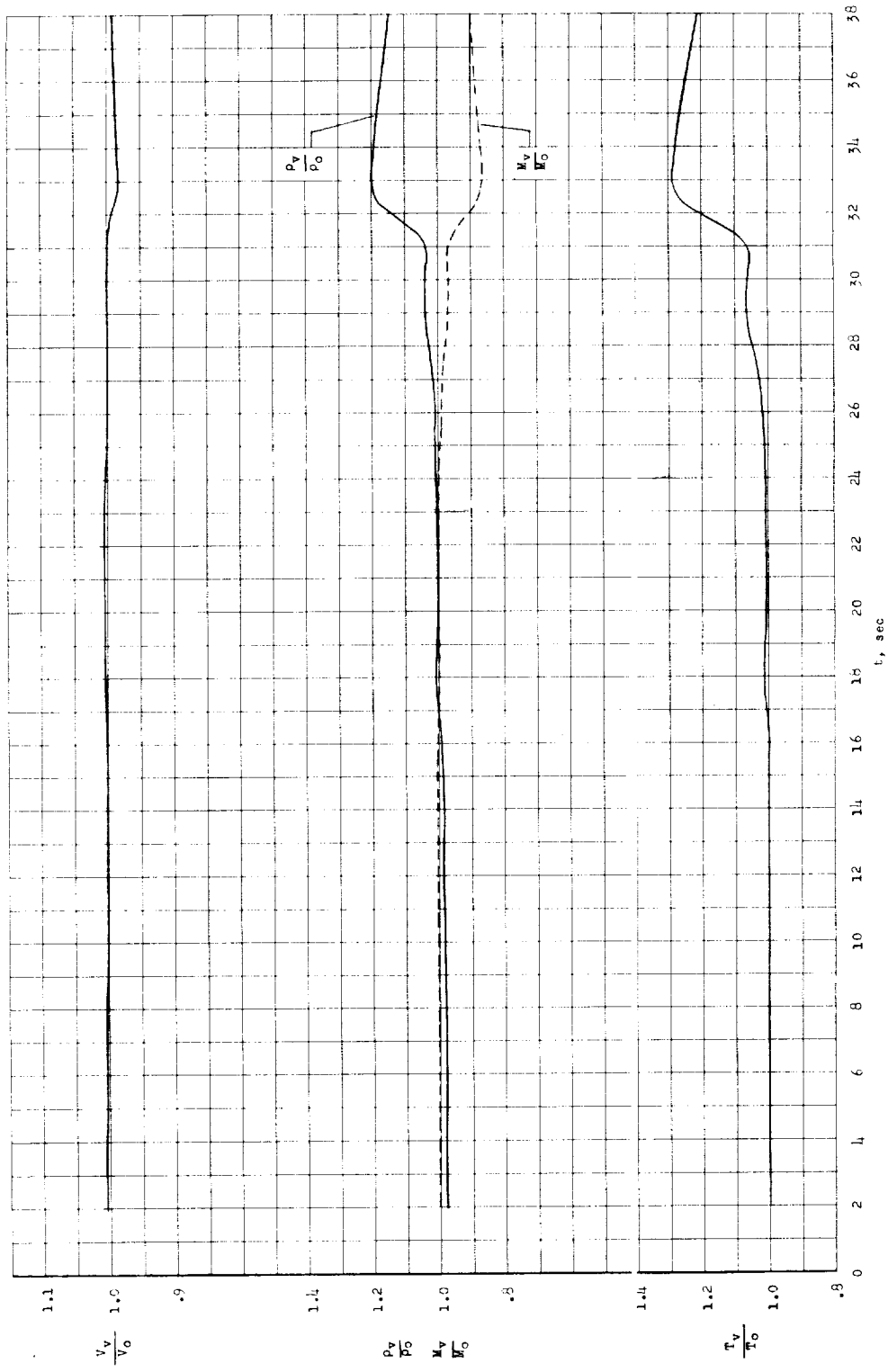

Figure 13.- Calculated flow parameters at the temperature measuring station.

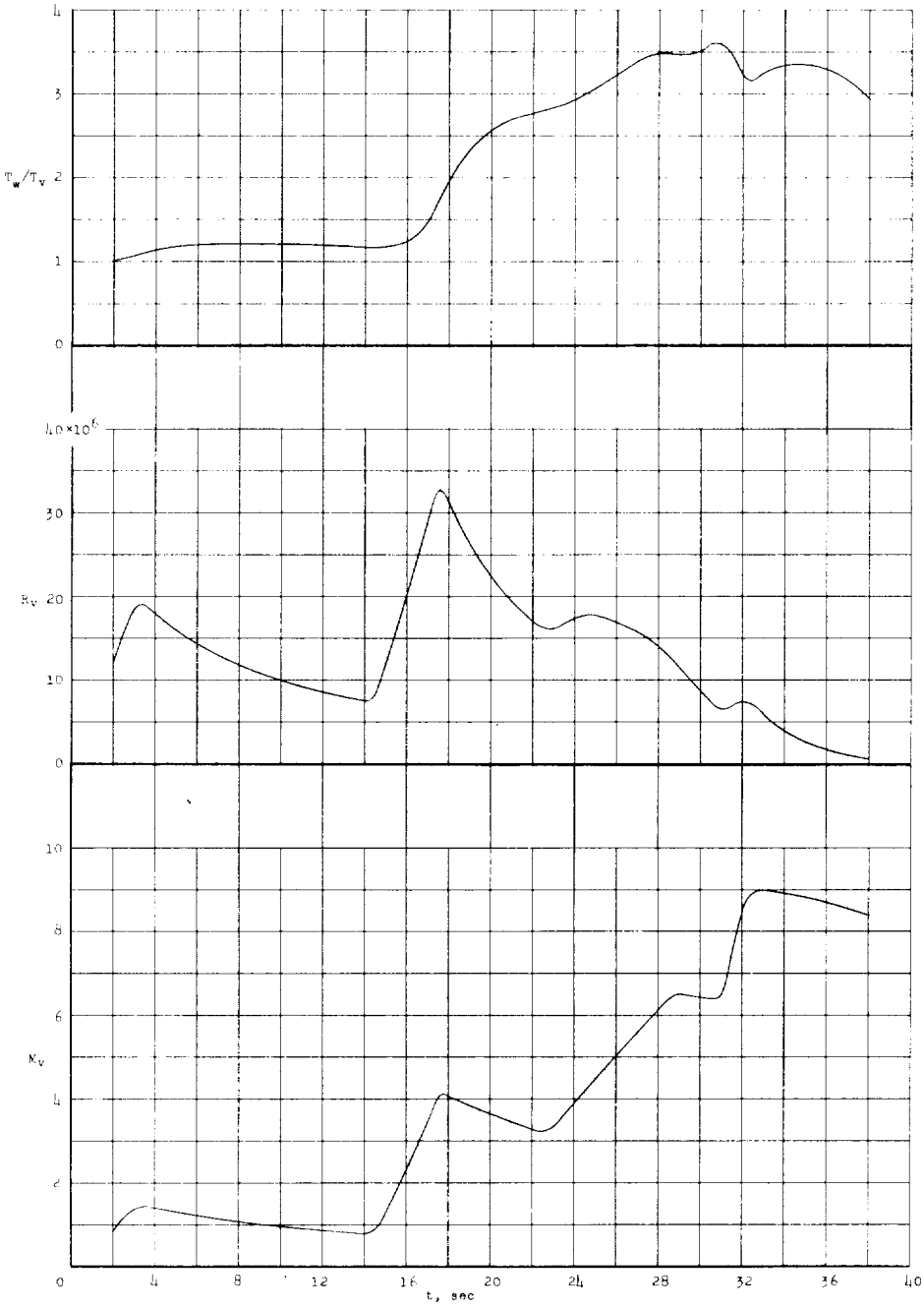

Figure 14.- Time histories of local Reynolds number based on axial distance to the temperature measuring station, local Mach number at the temperature measuring station, and ratio of wall temperature measured by thermocouple to local static temperature.

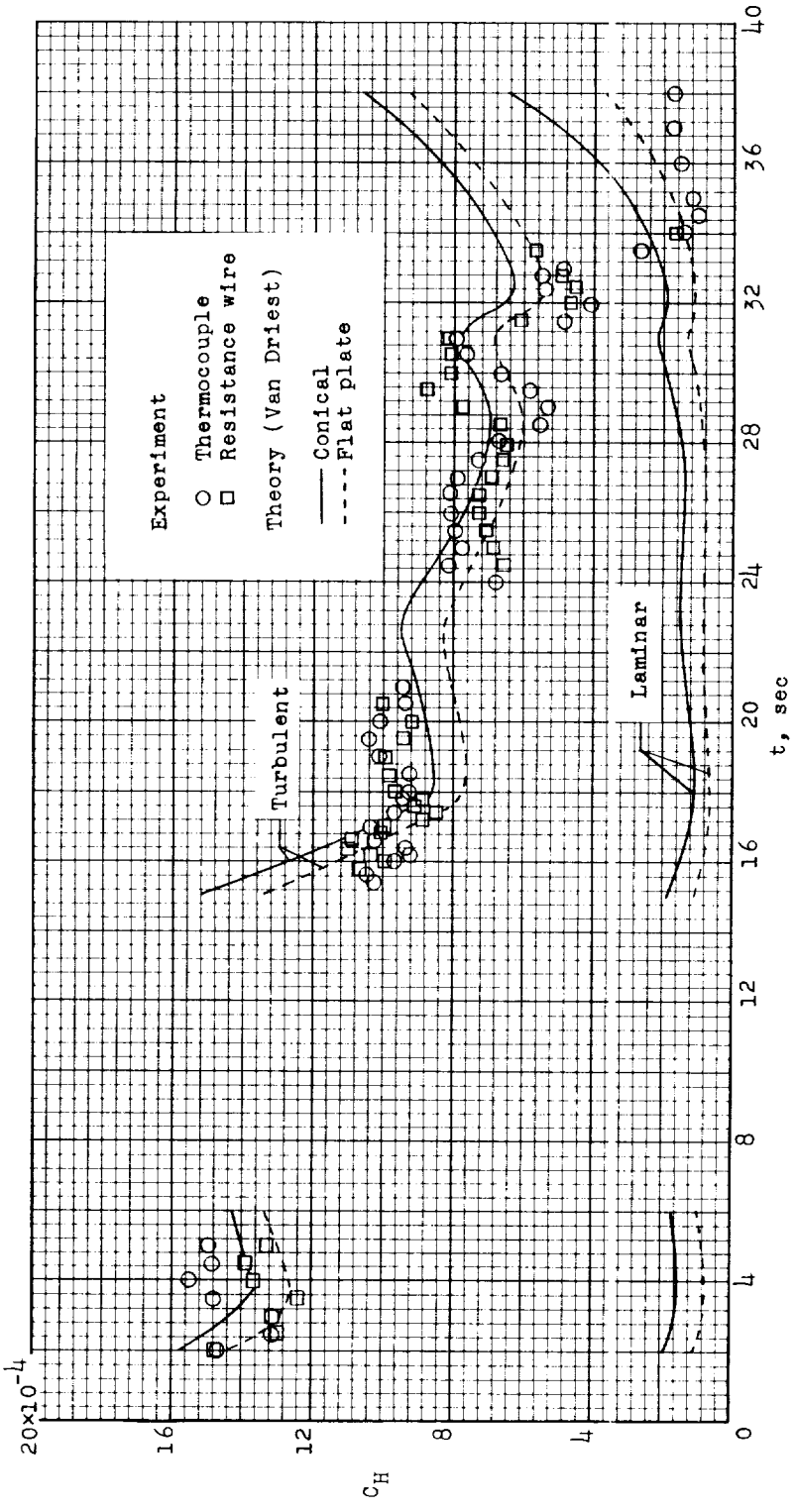

Figure 15.- Time histories of experimental and theoretical Stanton numbers.